
Article:
Wang, Junlin, Xia, Jing, Zhang, Xichao et al. (2020) Magnetic skyrmionium diode with a magnetic anisotropy voltage gating. Applied Physics Letters. 202401. ISSN: 0003-6951

https://doi.org/10.1063/5.0025124

Applied Physics Letters

Magnetic skyrmionium diode with a magnetic anisotropy voltage gating

Cite as: Appl. Phys. Lett. **117**, 202401 (2020); https://doi.org/10.1063/5.0025124
Submitted: 13 August 2020 . Accepted: 05 November 2020 . Published Online: 17 November 2020

Junlin Wang, Jing Xia, Xichao Zhang, Xiangyu Zheng, Guanqi Li, Li Chen, Yan Zhou, Jing Wu, Haihong Yin, Roy Chantrell, and Yongbing Xu

Applied Physics Letters ARTICLE scitation.org/journal/apl

Magnetic skyrmionium diode with a magnetic anisotropy voltage gating

Cite as: Appl. Phys. Lett. **117**, 202401 (2020); doi: 10.1063/5.0025124
Submitted: 13 August 2020 · Accepted: 5 November 2020 ·
Published Online: 17 November 2020

Junlin Wang,[1,2] Jing Xia,[3] Xichao Zhang,[2,3] Xiangyu Zheng,[1,2] Guanqi Li,[2,4] Li Chen,[5] Yan Zhou,[3,6,a)] Jing Wu,[2,4] Haihong Yin,[7] Roy Chantrell,[4] and Yongbing Xu[1,2,a)]

AFFILIATIONS

[1]Department of Electronic Engineering, University of York, York YO10 5DD, United Kingdom
[2]York-Nanjing International Center of Spintronics (YNICS), Nanjing University, Nanjing 210093, China
[3]School of Science and Engineering, The Chinese University of Hong Kong, Shenzhen, Guangdong 518172, China
[4]Department of Physics, University of York, York YO10 5DD, United Kingdom
[5]Faculty of Engineering, University of Leeds, Woodhouse Lane, Leeds LS2 9JT, United Kingdom
[6]Key Laboratory of Magnetic Molecules and Magnetic Information Materials of Ministry of Education, Linfen 041004, China
[7]School of Information Science and Technology, Nantong University, Nantong 226019, China

[a)]**Authors to whom correspondence should be addressed:** zhouyan@cuhk.edu.cn and yongbing.xu@york.ac.uk

ABSTRACT

The magnetic skyrmionium can be seen as a coalition of two magnetic skyrmions with opposite topological charges and has potential applications in next-generation spintronic devices. Here, we report the current-driven dynamics of a skyrmionium in a ferromagnetic nanotrack with the voltage-controlled magnetic anisotropy. The pinning and depinning of a skyrmionium controlled by the voltage gate are investigated. The current-driven skyrmionium can be used to mimic the skyrmionium diode effect in the nanotrack with a voltage gate. We have further studied the skyrmionium dynamics in the nanotrack driven by a magnetic anisotropy gradient in the absence of spin current. The performance of a single wedge-shaped voltage gate at different temperatures is studied. Our results may provide useful guidelines for the design of voltage-controlled and skyrmionium-based spintronic devices.

Magnetic skyrmions were predicted theoretically in 1989,[1] and since then, the creation, annihilation, and manipulation of magnetic skyrmions have been widely investigated in the field of magnetism and spintronics.[2–11] Magnetic skyrmions are particle-like nanoscale objects and can be found in certain ferromagnetic bulk materials, thin films, and multilayers,[2–11] where skyrmions are stabilized by a competition between the Heisenberg exchange interaction, Dzyaloshinskii–Moriya interaction (DMI), perpendicular magnetic anisotropy (PMA), and magnetic field. One of the most important applications of magnetic skyrmions is their use as information carriers in nanoscale spintronic devices,[7–11] where skyrmions can be driven by spin-transfer torques, spin–orbit torques, and spin waves. The skyrmion-based devices could have a lower power consumption or higher operation speed compared with the domain wall-based devices.[7–13]

However, the skyrmion Hall effect (SkHE)[14–16] could be an obstacle for the collimated transmission of skyrmions in narrow nanoscale devices.[17,18] The SkHE has been observed experimentally.[15,16] It is caused by the Magnus force acting on the moving skyrmion and can lead to the destruction of skyrmions at the device edges. One promising approach to avoid the SkHE is to create a topological spin texture with a zero net topological charge. For example, the synthetic antiferromagnetic bilayer skyrmion with a topological charge of $Q = 0$ is free from the SkHE.[17–20] In this system, the two exchange-coupled magnetic skyrmions in the top and bottom layers have opposite Q, leading to a total topological charge of zero.

On the other hand, a magnetic skyrmionium is also a topological spin texture with $Q = 0$.[21–39] It has a doughnut-like out-of-plane spin structure and can be seen as the combination of two skyrmions with opposite Q. The magnetic skyrmionium can be generated by ultra-fast laser pulses and has been observed experimentally[38] to be stable for over 12 months. Due to the zero topological charge, the magnetic skyrmionium is free from the SkHE. The dynamics of the skyrmionium have been studied theoretically[21–35] and observed in

experiments,[36–39] showing the potential of using skyrmioniums in next-generation spintronic devices.

In this work, we report a numerical study of current-induced skyrmionium dynamics in a ferromagnetic nanotrack with voltage-controlled perpendicular magnetic anisotropy (VCMA). The work performance of a nanotrack with a single voltage gate at different temperatures has also been studied, and the results show that the effect of voltage gate could be affected by the thermal effect. Our results show that a nanotrack with a voltage gate can be used to build a skyrmionium-based diode and ratchet memory. We found that the voltage gate-induced anisotropy gradient can realize the unidirectional motion of the skyrmionium in the nanotrack. We also study the dynamics of a skyrmionium driven by a PMA gradient, which has been observed in experiments and theoretically.[34,40] The simulation results of the skyrmionium driven by the anisotropy gradient without current demonstrate how the wedge shape voltage gate influences the magnetic skyrmionium motion in the nanotrack. PMA-gradient-induced skyrmionium motion can avoid the Joule heating effect, which may influence the stability of skyrmioniums. Our results are useful for the design of the voltage-controlled skyrmionium diode and the skyrmionium transport channel.

The simulation model is an ultra-thin ferromagnetic nanotrack of $1000 \times 180 \times 0.4$ nm^3, as shown in Fig. 1(a), which has interface-induced DMI and PMA. The mesh size is set as $2 \times 2 \times 0.4$ nm^3, which is small enough to ensure the numerical accuracy of the simulations. The micromagnetic simulations are performed using the Object Oriented MicroMagnetic Framework (OOMMF) package.[43] The dynamics of magnetization are governed by the Landau–Lifshitz–Gilbert (LLG) equation, written as

$$\frac{d\boldsymbol{m}}{dt} = -\gamma_0 \boldsymbol{m} \times \boldsymbol{h}_{\text{eff}} + \alpha\left(\boldsymbol{m} \times \frac{d\boldsymbol{m}}{dt}\right) - u\boldsymbol{m} \times (\boldsymbol{m} \times \boldsymbol{p}), \quad (1)$$

where the third term represents the spin torque arising from a spin polarized current. $\boldsymbol{m} = \boldsymbol{M}/M_S$ is the reduced magnetization and M_S is the saturation magnetization. γ_0 is the absolute value of the gyromagnetic ratio and α is the damping coefficient. $\boldsymbol{h}_{\text{eff}}$ is the effective field, including the contributions of Heisenberg exchange, DMI, PMA, and demagnetization. The parameter u is equal to $(\gamma_0 \hbar j \theta_{\text{SH}})/(2ae\mu_0 M_S)$, $\hbar$ is the reduced Plank constant, j is the applied current density, $\theta_{SH} = 0.08$ is the spin Hall angle, e is the electron charge, μ_0 is the vacuum permeability constant, and a is the thickness of the nanotrack. $\boldsymbol{p} = -\hat{y}$ is the spin polarization direction. Other magnetic material parameters are adopted from Ref. 28: $M_S = 580$ kA m^{-1}, ferromagnetic exchange constant $A = 15$ pJ m^{-1}, DMI constant $D = 3.5$ mJ m^{-2}, PMA constant $K_u = 0.8$ MJ m^{-3}, and $\alpha = 0.3$.

In our simulations, the setups of the voltage gate are illustrated in Fig. 1, where the PMA constant controlled by the voltage gate is defined as K_{uv}. First, in the study of the voltage-controlled pinning and depinning effects, a single wedge-shaped voltage gate is placed in the middle of and upon the ferromagnetic nanotrack [see Fig. 1(a)], which controls the PMA constant K_{uv} of the area underneath the voltage gate. We model the voltage-controlled PMA constant $K_v(x)$ as a linear function of the longitudinal coordinate x and the default PMA constant K_u as follows: $K_v(x) = K_u + (K_{uv} - K_u)(x - x_0)/l$ for $x \in [x_0, x_0 + l]$, where l is the length of the voltage gate, K_{uv} is the maximum PMA induced by the voltage, and x_0 denotes the location of the voltage gate.

Second, in order to study the voltage-gradient-induced skyrmionium motion, as shown in Fig. 1(b), a wedge-shaped voltage gate is placed upon the whole ferromagnetic nanotrack, leading to varying PMA $K_v(x)$ along the x direction. We again model the PMA constant $K_v(x)$ as a linear function, this time over the whole track, of the longitudinal coordinate x and the default PMA constant K_u, specifically $K_v(x) = K_u + (K_{uv} - K_u)x/l$ for $x \in [x_0, x_0 + l]$. Note that when studying the skyrmionium driven by the VCMA gradient along the x direction, no other external driving force, such as the spin current, is applied. For the initial state of all simulations, a relaxed skyrmionium is placed at the left or right end of the ferromagnetic nanotrack, which is then driven by the spin current or VCMA gradient.

The pinning and depinning states of the current-driven skyrmionium in the nanotrack with a local wedge-shaped voltage gate are shown in Fig. 2. The effects of the voltage gate length l and current density j on the skyrmionium motion are given in Figs. 2(a) and 2(b), respectively. The relaxed skyrmionium is placed near the left end of the nanotrack as the initial state for Fig. 2(a). When a driving current is applied along the $+x$ direction in the heavy-metal layer, a damping-like spin–orbit torque is generated to drive the magnetization dynamics in the ferromagnetic nanotrack. Consequently, the skyrmionium moves toward the left side of the VCMA region. Due to the VCMA in the nanotrack, only a current larger than a certain threshold can drive the skyrmionium through the voltage-gated region from the left to the right side. The reason is that the PMA gap in the ferromagnetic

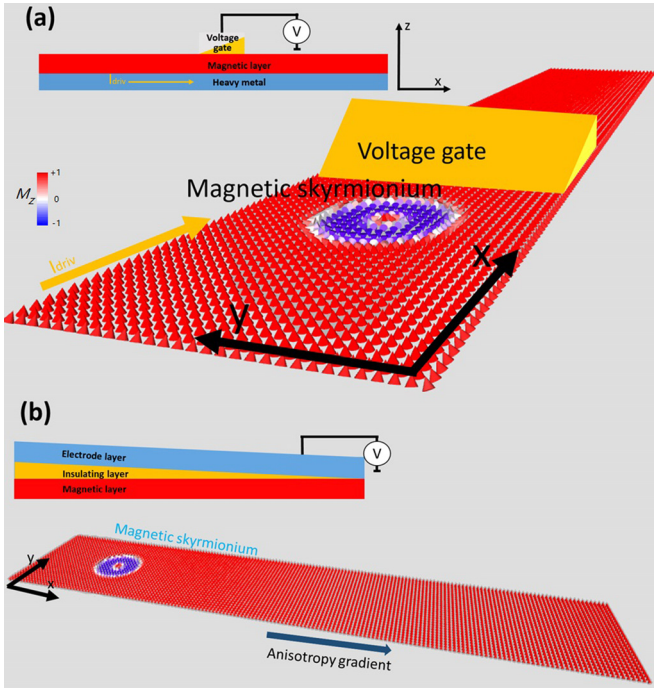

FIG. 1. (a) Illustration of the skyrmionium-based device controlled by a gate voltage. The out-of-plane magnetization component (m_z) is color coded: red means $m_z = +1$, white means $m_z = 0$, and blue means $m_z = -1$. (b) The skyrmionium driven by the voltage-controlled magnetic anisotropy (VCMA) gradient in a ferromagnetic nanotrack.

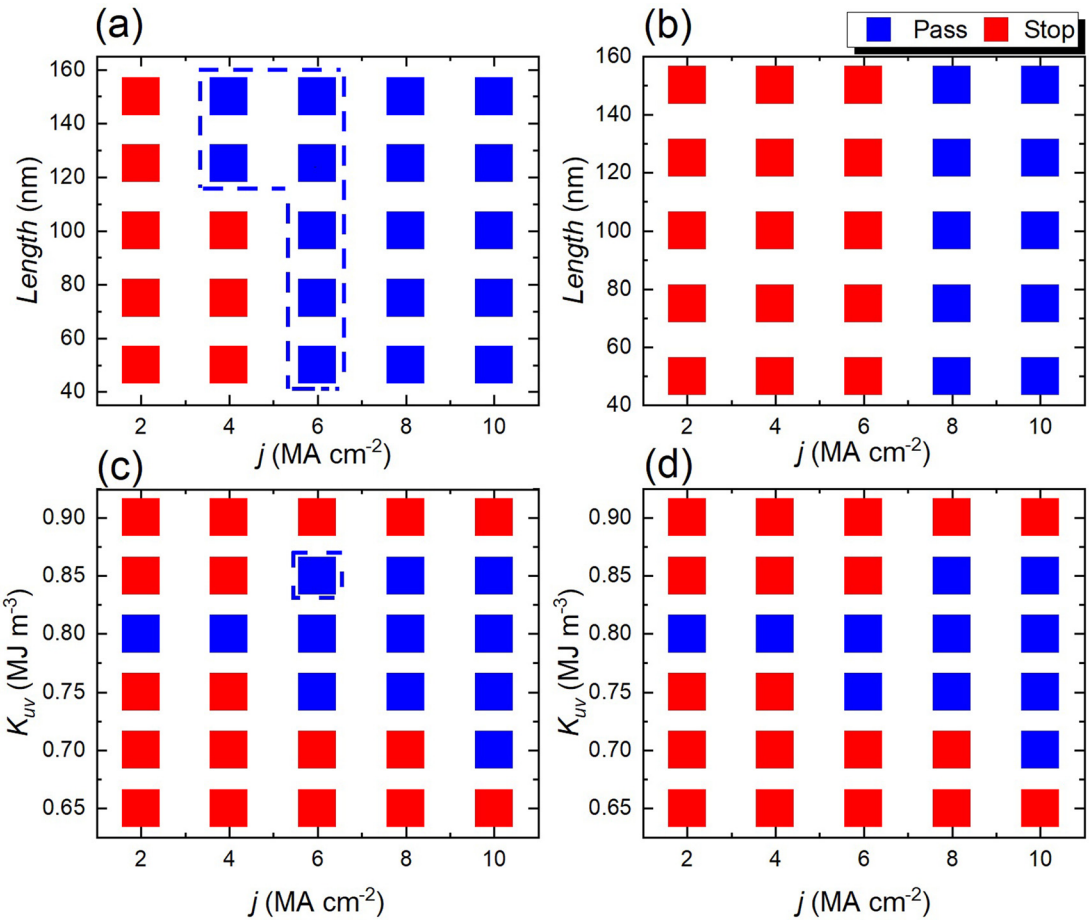

FIG. 2. The pinning and depinning states of an isolated skyrmionium driven by the spin current in a ferromagnetic nanotrack with a single wedge-shaped voltage gate. The solid red squares denote that the skyrmionium is pinned by the VCMA region, and the solid blue squares denote that the skyrmionium passes the VCMA region. The dotted blue lines indicate areas of unidirectional skyrmionium motion. (a) The pinning and depinning states of a skyrmionium with various lengths l from 50 nm to 150 nm and various driving current densities j from 2 MA cm^{-2} to 10 MA cm^{-2}. The driving current is applied along the $+x$ direction. $K_{uv} = 0.85$ MJ m^{-3}. (b) The driving current is applied along the $-x$ direction. $K_{uv} = 0.85$ MJ m^{-3}. (c) The pinning and depinning states of a skyrmionium with various K_{uv} from 0.65 MJ m^{-3} to 0.90 MJ m^{-3} and various j from 2 MA cm^{-2} to 10 MA cm^{-2}. The driving current is applied along the $+x$ direction. $l = 100$ nm. (d) The driving current is applied along the $-x$ direction. $l = 100$ nm.

nanotrack, which is defined as $K_{gap} = K_{uv} - K_u$ in this work, leads to an energy barrier for the skyrmionium motion. The precise anisotropy profile along the nanotrack is given in the supplementary material.

As shown in Fig. 2(a), a VCMA region with a length l smaller than 125 nm can pin the skyrmionium when the driving current density j is smaller than 6 MA cm^{-2}. When the length l is larger than 125 nm, a current-driven skyrmionium can pass the VCMA region with a current $j \geq 4$ MA cm^{-2}, which indicates that the pinning and depinning states can be affected by the slope of the VCMA gradient. Namely, a longer VCMA gate length, and consequently reduced gradient, can lower the threshold depinning current density.

In Fig. 2(b), a relaxed skyrmionium is initially located near the right end of the nanotrack and a driving current along the $-x$ direction is applied. The skyrmionium moves along the $-x$ direction and toward the right side of the VCMA region. When the driving current density j is smaller than 8 MA cm^{-2}, the skyrmionium is pinned by the VCMA region. The pinning and depinning states of the skyrmionium are independent of the length of the VCMA region.

Compared with Fig. 2(a), the right boundary of the VCMA region induces a very high and sharp PMA energy barrier K_{gap}, which is hard for the skyrmionium to overcome. The blue dashed box in Fig. 2 indicates the cases in which the skyrmionium displays unidirectional motion along the nanotrack, which provide information for realizing a skyrmionium-based diode device.

In Figs. 2(c) and 2(d), the effects of the different K_{uv} and current density j are given, respectively. The pinning and depinning states are sensitive to K_{uv} of the VCMA region. The parameters for the unidirectional motion along the $+x$ direction have been marked in a blue dashed box. When $|K_{gap}| \geq 0.10$ MJ m^{-3}, the skyrmionium is difficult to drive through the VCMA region because a larger K_{gap} leads to a larger energy barrier. From Fig. 2, under the same driving current density, a larger K_{gap} is more likely to result in the pinning of the

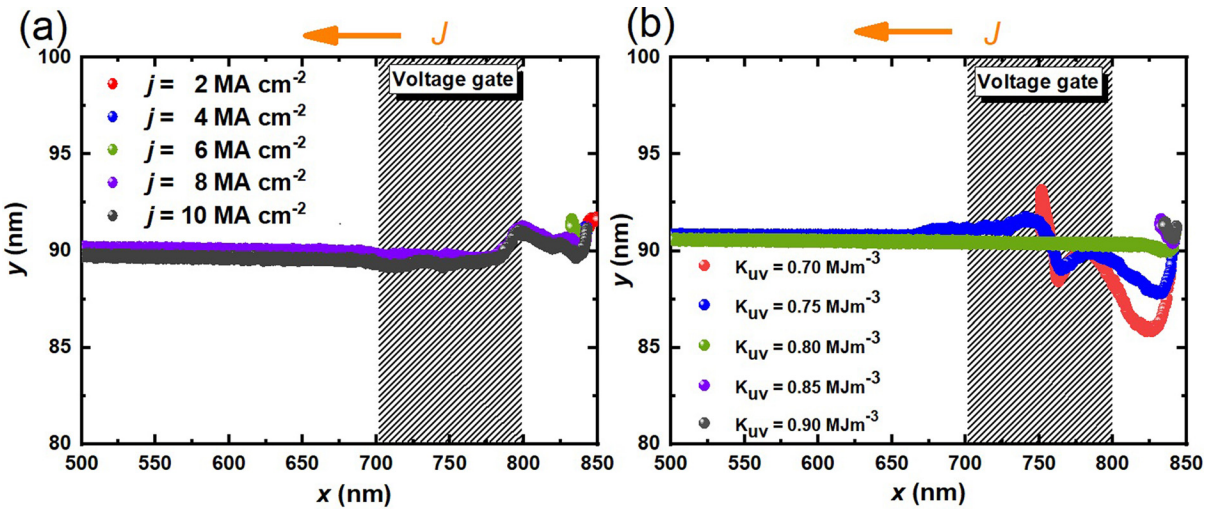

FIG. 3. (a) The trajectory of a skyrmionium in the nanotrack driven by a current density j varying from 2 MA cm^{-2} to 10 MA cm^{-2}. $K_{uv} = 0.85$ MJ m^{-3} and the voltage gate area is located at $x = 700$ nm with $l = 100$ nm. (b) The trajectory of a skyrmionium in the nanotrack driven by a current density j of 6 MA cm^{-2}. K_{uv} varies from 0.70 to 0.85 MJ m^{-3}, and the voltage gate area is located at $x = 700$ nm with $l = 100$ nm.

skyrmionium by the VCMA region. The simulation results obtained with a smaller current density step are given in the supplementary material.

The trajectories of a skyrmionium moving along the $-x$ direction in the nanotrack with a single voltage gate are shown in Fig. 3. The driving current density in Fig. 3(a) is varied from 2 MA cm^{-2} to 10 MA cm^{-2}. It can be seen that when the driving current is lower than the threshold value, the skyrmionium is pinned at the right boundary of the VCMA region. When the current density increases, the pinned skyrmionium moves closer to the boundary until the current density is large enough to drive the skyrmionium through the VCMA region. The skyrmionium passing through the right boundary of the VCMA region can be seen as the diode breakdown effect of this skyrmionium-based device.

Furthermore, the slope-shaped VCMA region will enhance the velocity of the skyrmionium on passing through the VCMA region. The VCMA gradient can also cause a small deformation of the skyrmionium because of the SkHE and varying PMA, which also affects the skyrmionium trajectory. This phenomenon is demonstrated in Fig. 3(a), when the driving current density j is larger than 6 MA cm^{-2}.

The trajectories of a skyrmionium driven by a current density of 6 MA cm^{-2} for different VCMA gradients are shown in Fig. 3(b). When $K_{gap} < 0$ and the skyrmionium moves from the high PMA region to low PMA region, the VCMA region could increase the velocity of the skyrmionium and cause a deformation of the skyrmionium. If the driving current density is lower than the threshold value, the skyrmionium is pinned inside the VCMA region. For the case of $K_{gap} > 0$, the skyrmionium is pinned at the right boundary of the VCMA region if the driven current is lower than the threshold.

The spin configurations of a skyrmionium pinned in the nanotrack with $K_{gap} > 0$ and $K_{gap} < 0$ are given in Fig. 4, along with the pinning position of the skyrmionium at different K_{uv}. In Figs. 4(a) and 4(b), the skyrmionium can enter the VCMA region easily because the K_{uv} is lower than K_u. After the skyrmionium has moved into the VCMA region, the skyrmionium will deform due to the decrease in PMA and if the polarized current is not large enough, the skyrmionium will be pinned at the left boundary of the VCMA region. For the case of $K_{uv} > K_u$ in Figs. 4(c) and 4(d), if the driven current density is not large enough, the skyrmionium will be pinned at the right

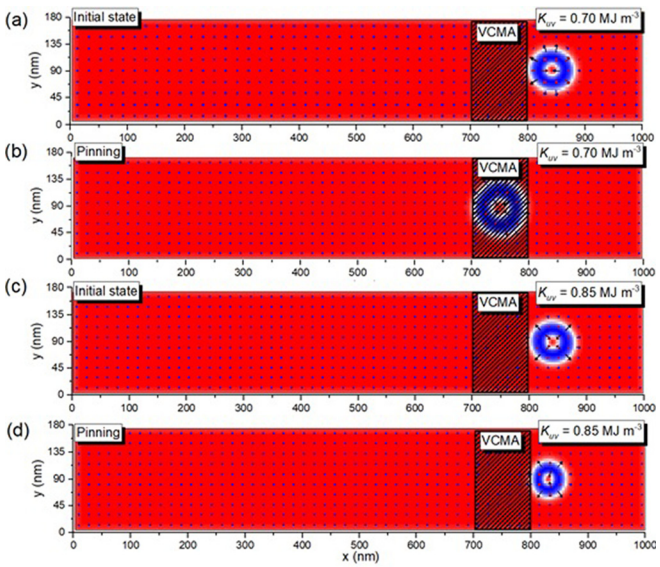

FIG. 4. The spin configuration of an isolated skyrmionium driven by the spin current as 6 MA cm^{-2} motion toward left in a ferromagnetic nanotrack with a single wedge-shaped voltage gate. (a) The initial state of the isolated skyrmionium in a nanotrack with a wedge-shaped voltage gate with a K_{uv} as 0.70 MJ m^{-3}. (b) The isolate skyrmionium pinned after entry into the VCMA region. (c) The initial state of the isolated skyrmionium in a nanotrack with a wedge-shaped voltage gate with a K_{uv} as 0.85 MJ m^{-3}. (d) The isolated skyrmionium pinned before entry the VCMA region.

boundary of the VCMA region. Then, the increased PMA and driving current will induce deformation of the skyrmionium.

In addition, the spin configurations of a skyrmionium diode device at different temperatures are given in Fig. 5. The micromagnetic simulation including the thermal effect is simulated by the OOMMF extensible solver (OXS) object.[41] The time step in the simulation with the thermal effect is fixed at 10 fs, and the temperature changes from 50 K to 75 K. In Figs. 5(a) and 5(b), the skyrmionium can be driven through the VCMA region by the spin polarized current at 0 K. However, the thermal fluctuation in the system will decrease the effective magnetic anisotropy, DMI, and exchange interaction, which will induce a deformation of the skyrmionium as shown in Figs. 5(c) and 5(d).[42] On the other hand, the energy barrier between K_{uv} and K_u in the VCMA region will also be reduced, which will influence the skyrmionium behavior in the VCMA region. In Figs. 5(e)–5(g), the skyrmionium is pinned by the VCMA region because the current density is not large enough. Then in Fig. 5(h), when the temperature is high enough, the energy barrier between K_{uv} and K_u will reduce to a smaller value, which makes the current density large enough to drive the skyrmionium through the VCMA region. In Fig. S3 of the supplementary material, the simulation results also show the same phenomenon with a larger K_{uv}. From the results in Figs. 5 and S3, it is found that the skyrmionium-based diode is sensitive to the thermal effect. If the applied thermal field is larger than a threshold, the reduced energy barrier between K_{uv} and K_u will break the unidirectional function of the skyrmionium diode device. The simulation results show that the skyrmionium diode works well even under a weak thermal condition. If the thermal fluctuation is too strong, the unidirectional motion behavior of the skyrmionium will disappear and the skyrmionium will be deformed. These results show that the skyrmionium transmission channel can be controlled by the VCMA effect and can mimic the field-effect transistor (FET) device.

The magnetic skyrmionium/skyrmion motion in a nanowire induced by a current pulse are next studied and compared. The trajectories of the skyrmion/skyrmionium driven by a pulse current in a nanotrack with the VCMA gate are given in Fig. 6. When the current pulse is on, the skyrmionium is driven by the current and moves through the VCMA region. But in this case, the driving current pulse time and current density are not large enough to make the skyrmionium move through the VCMA region. If the current pulse is removed, the gradient of the VCMA gate will drive the skyrmionium toward the left side of the nanotrack. The magnetic skyrmionium is free from the SkHE and has a linear trajectory as shown in Fig. 6(a): under the influence of a driving current, the skyrmionium moves in a straight line along the nanotrack. For the skyrmion case, the trajectory is much more complex as shown in Fig. 6(b). When the current pulse is on, the skyrmion has a velocity toward the top of the nanotrack, which comes from the SkHE until there is a balance between the edge force and the SkHE. Under the action of these forces, the skyrmion moves along the track direction but with oscillatory motion in the y-direction. Then, if the current pulse is turned off, the VCMA gradient of the gate will make the skyrmion move toward the left side of the nanotrack. The skyrmion has a large velocity toward the bottom of the nanowire, which is a combination of edge force and the SkHE. From the simulation results, the trajectories of the skyrmionium and skyrmion in a nanowire with the VCMA gate driven by the current pulse are significantly different. The current/current pulse-driven skyrmionium motion in the nanotrack with the VCMA gate is retained in the middle of the nanowire and avoids destruction at the edge. The trajectory shows that a skyrmion and

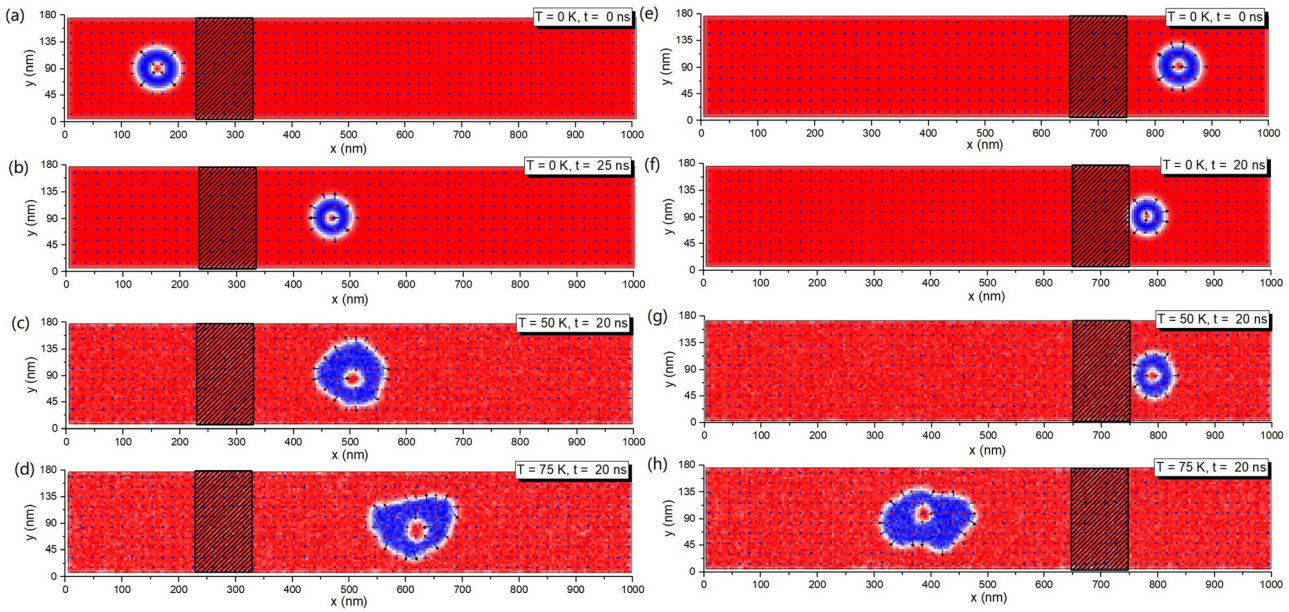

FIG. 5. The spin configurations of an isolated skyrmionium driven by the spin current j = 5 MA cm^{-2} in a ferromagnetic nanotrack with a single wedge-shaped voltage gate with a K_{uv} = 0.85 MJ m^{-3} at different temperatures. (a) The initial state of the skyrmionium moves toward the $+x$ direction at 0 ns under 0 K. (b) t = 25 ns, T = 0 K. (c) t = 20 ns, T = 50 K. (d) t = 20 ns, T = 75 K. (e) The initial state of the skyrmionium moves toward the $-x$ direction at 0 ns under 0 K. (f) t = 20 ns, T = 0 K. (g) t = 20 ns, T = 50 K. (h) t = 20 ns, T = 75 K.

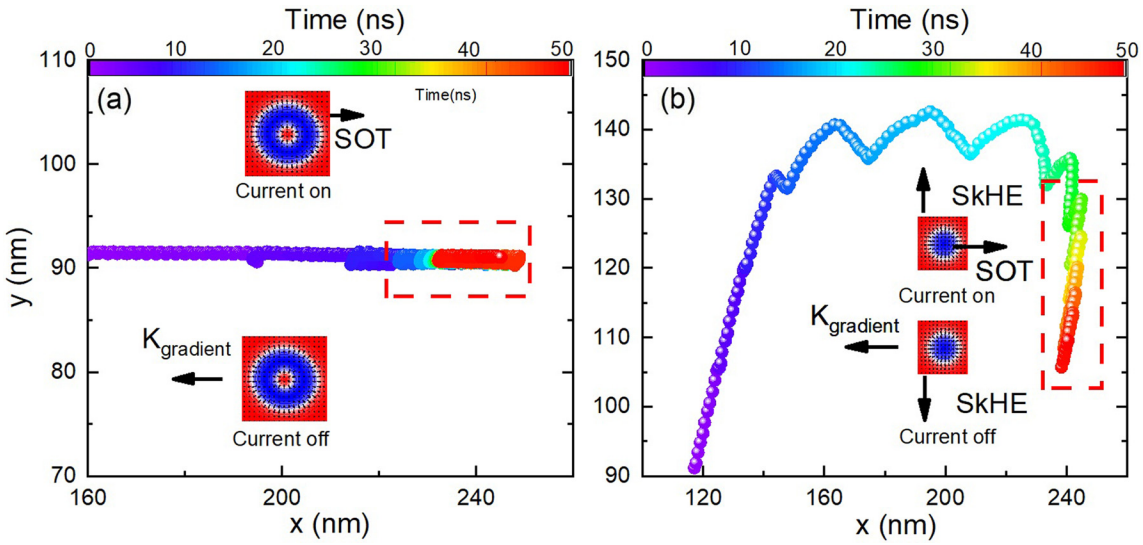

FIG. 6. The trajectory of the magnetic skyrmionium and skyrmion driven by pulse current. The current duration is 2 ns, and there is a 2-ns delay between two current pulses. The skyrmionium and skyrmion move toward the right side of the nanotrack, and the total simulation time is 50 ns, which is indicated by the color bar. (a) The trajectory of the magnetic skyrmionium in the nanotrack with the VCMA gate driven by current pulses. (b) The trajectory of the magnetic skyrmion in the nanotrack with the VCMA gate driven by current pulses.

skyrmionium can be driven by an anisotropy gradient without current or other external driving force.

The motion of magnetic skyrmions driven by a PMA gradient has been studied recently.[40,44] A skyrmion moves toward the area with a lower PMA. Similar to a skyrmion, a skyrmionium also moves toward the area with a lower PMA. From the simulation results in Fig. 6, the skyrmionium tends to move from the high-PMA region to the lower-PMA region when no driving current is applied. In this work, we also study the skyrmionium motion driven by a VCMA gradient [see Fig. 1(b)]. The velocities of the skyrmionium driven by different PMA gradients are given in Fig. S4, and the spin configuration of skyrmionium driven by the VCMA gradient in the nanotrack is given in Fig. S5 in the supplementary material. It can be seen that the velocities of the skyrmionium at different PMA gradients have a similar trend and depend on the amplitude of the PMA gradient. The distortion of the skyrmionium induced by the anisotropy gradient may reduce the stability of the skyrmionium when it is close to the sample edge.

In conclusion, we have studied the motion of a skyrmionium in a ferromagnetic nanotrack with the PMA gradient controlled by a gate voltage. Our simulation results show that the trajectory and velocity of the skyrmionium can be controlled by a wedge-shaped voltage gate. The unidirectional motion of the skyrmionium realized by the VCMA effect can be used to build a skyrmionium-based one-way information channel, that is, the skyrmionium diode. The skyrmionium-based information channel can be controlled by the VCMA effect and can mimic the FET function. A skyrmionium driven by a current pulse in the nanotrack with a VCMA gate has a different trajectory to that of a skyrmion, which shows that the skyrmionium-based information channel is free from the effects of an edge defect. We further numerically demonstrated that the PMA gradient can be used to drive the motion of a skyrmionium in a nanotrack in the absence of a driving current. Our results, and the basic principles demonstrated, are likely to prove useful for the design and development of future skyrmionium-based information storage and processing devices.

See the supplementary material for more results about the anisotropy profile in the nanotrack, the simulation results obtained with a smaller current density step, spin configurations of an isolated skyrmionium driven by the spin current in a ferromagnetic nanotrack with a single wedge-shaped voltage gate at different temperatures, the velocities of the skyrmionium driven by different PMA gradients, and the spin configuration of the skyrmionium driven by the VCMA gradient in the nanotrack.

This work was supported by the State Key Program for Basic Research of China (Grant No. 2016YFA0300803), the National Natural Science Foundation of China (Grant Nos. 61427812 and 11574137), the Jiangsu Natural Science Foundation (Grant No. BK20140054), the Jiangsu Shuangchuang Team Program, and the UK EPSRC (No. EP/G010064/1). X.Z. acknowledges the support from the National Natural Science Foundation of China (Grant No. 12004320) and the Guangdong Basic and Applied Basic Research Foundation (Grant No. 2019A1515110713). Y.Z. acknowledges the support from the President's Fund of CUHKSZ, Longgang Key Laboratory of Applied Spintronics, National Natural Science Foundation of China (Grant Nos. 11974298 and 61961136006), Shenzhen Key Laboratory Project (Grant No. ZDSYS201603311644527), and Shenzhen Peacock Group Plan (Grant No. KQTD20180413181702403).

DATA AVAILABILITY

The data that support the findings of this study are available from the corresponding authors upon reasonable request.

REFERENCES

[1]A. N. Bogdanov and D. A. Yablonskii, Sov. Phys. JETP **68**, 101 (1989); available at http://www.jetp.ac.ru/cgi-bin/e/index/e/68/1/p101?a=list.
[2]N. Nagaosa and Y. Tokura, Nat. Nanotechnol. **8**, 899 (2013).
[3]R. Wiesendanger, Nat. Rev. Mater. **1**, 16044 (2016).
[4]N. Kanazawa, S. Seki, and Y. Tokura, Adv. Mater. **29**, 1603227 (2017).
[5]W. Jiang, G. Chen, K. Liu, J. Zang, S. G. Velthuiste, and A. Hoffmann, Phys. Rep. **704**, 1 (2017).
[6]K. Everschor-Sitte, J. Masell, R. M. Reeve, and M. Kläui, J. Appl. Phys. **124**, 240901 (2018).
[7]W. Kang, Y. Huang, X. Zhang, Y. Zhou, and W. Zhao, Proc. IEEE **104**, 2040 (2016).
[8]A. Fert, N. Reyren, and V. Cros, Nat. Rev. Mater. **2**, 17031 (2017).
[9]Y. Zhou, Natl. Sci. Rev. **6**, 210 (2019).
[10]G. Finocchio, F. Büttner, R. Tomasello, M. Carpentieri, and M. Kläui, J. Phys. D **49**, 423001 (2016).
[11]X. Zhang, Y. Zhou, K. M. Song, T.-E. Park, J. Xia, M. Ezawa, X. Liu, W. Zhao, G. Zhao, and S. Woo, J. Phys. **32**, 143001 (2020).
[12]S. Parkin, M. Hayashi, and L. Thomas, Science **320**, 190 (2008).
[13]X. Zheng, J. Wang, G. Li, X. Lu, W. Li, Y. Wang, L. Chen, H. Yin, J. Wu, and Y. Xu, ACS Appl. Electron. Mater. **2**, 2375 (2020).
[14]J. Zang, M. Mostovoy, J. H. Han, and N. Nagaosa, Phys. Rev. Lett. **107**, 136804 (2011).
[15]W. Jiang, X. Zhang, G. Yu, W. Zhang, X. Wang, M. Benjamin Jungfleisch, J. E. Pearson, X. Cheng, O. Heinonen, K. L. Wang, Y. Zhou, A. Hoffmann, and S. G. E. Velthuiste, Nat. Phys. **13**, 162 (2017).
[16]K. Litzius, I. Lemesh, B. Kruger, P. Bassirian, L. Caretta, K. Richter, F. Buttner, K. Sato, O. A. Tretiakov, J. Forster, R. M. Reeve, M. Weigand, I. Bykova, H. Stoll, G. Schutz, G. S. D. Beach, and M. Klaui, Nat. Phys. **13**, 170 (2017).
[17]X. Zhang, Y. Zhou, and M. Ezawa, Nat. Commun. **7**, 10293 (2016).
[18]X. Zhang, M. Ezawa, and Y. Zhou, Phys. Rev. B **94**, 064406 (2016).
[19]T. Dohi, S. DuttaGupta, S. Fukami, and H. Ohno, Nat. Commun. **10**, 5153 (2019).
[20]W. Legrand, D. Maccariello, F. Ajejas, S. Collin, A. Vecchiola, K. Bouzehouane, N. Reyren, V. Cros, and A. Fert, Nat. Mater. **19**, 34 (2020).
[21]A. Bogdanov and A. Hubert, J. Magn. Magn. Mater. **195**, 182 (1999).
[22]S. Rohart and A. Thiaville, Phys. Rev. B **88**, 184422 (2013).
[23]A. O. Leonov, U. K. Rößler, and M. Mostovoy, EPJ Web Conf. **75**, 05002 (2014).
[24]M. Beg, R. Carey, W. Wang, D. Cortés-Ortuño, M. Vousden, M.-A. Bisotti, M. Albert, D. Chernyshenko, O. Hovorka, R. L. Stamps, and H. Fangohr, Sci. Rep. **5**, 17137 (2015).
[25]S. Komineas and N. Papanicolaou, Phys. Rev. B **92**, 064412 (2015).
[26]X. Liu, Q. Zhu, S. Zhang, Q. Liu, and J. Wang, AIP Adv. **5**, 087137 (2015).
[27]Y. Liu, H. Du, M. Jia, and A. Du, Phys. Rev. B **91**, 094425 (2015).
[28]X. Zhang, J. Xia, Y. Zhou, D. Wang, X. Liu, W. Zhao, and M. Ezawa, Phys. Rev. B **94**, 094420 (2016).
[29]H. Fujita and M. Sato, Phys. Rev. B **95**, 054421 (2017).
[30]A. G. Kolesnikov, M. E. Stebliy, A. S. Samardak, and A. V. Ognev, Sci. Rep. **8**, 16966 (2018).
[31]S. Li, J. Xia, X. Zhang, M. Ezawa, W. Kang, X. Liu, Y. Zhou, and W. Zhao, Appl. Phys. Lett. **112**, 142404 (2018).
[32]M. Shen, Y. Zhang, J. Ou-Yang, X. Yang, and L. You, Appl. Phys. Lett. **112**, 062403 (2018).
[33]B. Göbel, A. F. Schäffer, J. Berakdar, I. Mertig, and S. S. P. Parkin, Sci. Rep. **9**, 12119 (2019).
[34]C. Song, C. Jin, J. Wang, Y. Ma, H. Xia, J. Wang, J. Wang, and Q. Liu, Appl. Phys. Express **12**, 083003 (2019).
[35]L. Bo, R. Zhao, C. Hu, Z. Shi, W. Chen, X. Zhang, and M. Yan, J. Phys. D **53**, 195001 (2020).
[36]R. Streubel, L. Han, M.-Y. Im, F. Kronast, U. K. Rößler, F. Radu, R. Abrudan, G. Lin, O. G. Schmidt, P. Fischer, and D. Makarov, Sci. Rep. **5**, 8787 (2015).
[37]S. Zhang, F. Kronast, G. van der Laan, and T. Hesjedal, Nano Lett. **18**, 1057 (2018).
[38]M. Finazzi, M. Savoini, A. R. Khorsand, A. Tsukamoto, A. Itoh, L. Duò, A. Kirilyuk, T. Rasing, and M. Ezawa, Phys. Rev. Lett. **110**, 177205 (2013).
[39]F. Zheng, H. Li, S. Wang, D. Song, C. Jin, W. Wei, A. Kovács, J. Zang, M. Tian, Y. Zhang, H. Du, and R. E. Dunin-Borkowski, Phys. Rev. Lett. **119**, 197205 (2017).
[40]C. Ma, X. Zhang, J. Xia, M. Ezawa, W. Jiang, T. Ono, S. N. Piramanayagam, A. Morisako, Y. Zhou, and X. Liu, Nano Lett. **19**, 353 (2019).
[41]See http://kelvinxyfong.wordpress.com/research/research-interests/oommfex-tensions/oommf-extension-xf_thermspinxferevolve for "The OOMMF OXS Extension Module of the Spin-Transfer Torque and Thermal Fluctuation Effect."
[42]R. Tomasello, K. Y. Guslienko, M. Ricci, A. Giordano, J. Barker, M. Carpentieri, O. Chubykalo-Fesenko, and G. Finocchio, Phys. Rev. B **97**, 060402 (2018).
[43]M. J. Donahue and D. G. Porter, "OOMMF user's guide, version 1.0," Interagency Report No. NISTIR 6376 (NISTIR, 1999).
[44]H. Xia, C. Song, C. Jin, J. Wang, J. Wang, and Q. Liu, J. Magn. Magn. Mater. **458**, 57 (2018).